JCTC Journal of Chemical Theory and Computation

pubs.acs.org/JCTC Article

Quantum-Chemical and Quantum-Graph Models of the Dynamical Structure of CH_5^+

Irén Simkó, Csaba Fábri, and Attila G. Császár*

Cite This: J. Chem. Theory Comput. 2023, 19, 42−50 Read Online

ACCESS | Metrics & More | Article Recommendations | Supporting Information

ABSTRACT: Experimental and computational results about the structure, dynamics, and rovibrational spectra of protonated methane have challenged a considerable number of traditional chemical concepts. Hereby theoretical and computational results are provided about the dynamical structure of CH_5^+. It is shown that the ground vibrational state investigated thus far by computations, forbidden by nuclear-spin statistics, has a structure similar to the first allowed vibrational state and, in fact, the structures of all vibrational states significantly below 200 cm^{-1} are highly similar. Spatial delocalization of the nuclei, determined by nuclear densities computed from accurate variational vibrational wave functions, turns out to be limited when viewed in the body-fixed frame, confirming that the effective structure of CH_5^+ is well described as a CH_3^+ tripod with a H_2 unit on top of it. The interesting and unusual qualitative aspects of the sophisticated state-dependent variational results receive full explanation via simple quantum-graph models.

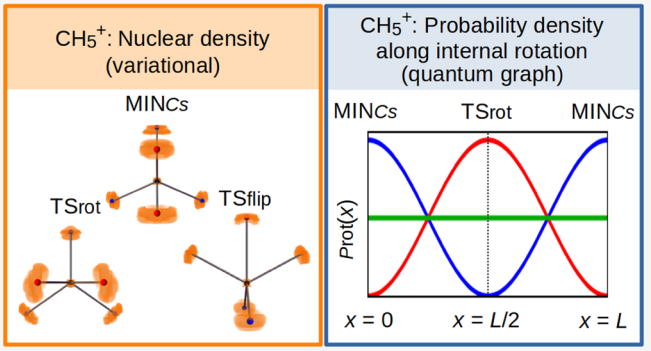

1. INTRODUCTION

Protonated methane, that is the CH_5^+ molecular cation, is one of the founding parents of the family of quasistructural molecules.[1] The unusual structure,[2−6] stability,[7] and nuclear dynamics,[2,8] as well as the congested high-resolution spectra[9−14] of CH_5^+, and its (deuterated) isotopologues, have been interrogated not only experimentally but also via a number of computational techniques, such as ab initio path integral molecular dynamics (PIMD),[2] diffusion quantum Monte Carlo (DQMC),[8,15−19] (multilayer) multiconfigurational time-dependent Hartree (MCTDH),[20] and nearly exact variational solutions[11,21−23] of the time-independent nuclear Schrödinger equation.

The three most important stationary points (SP)[24] on the ground-electronic-state potential energy surface (PES) of CH_5^+ are given in Figure 1. Not only the electronic energies but also the rotational constants of these SPs are very similar. The equilibrium structure of the global minimum, here called MIN_{C_s}, has C_s point-group symmetry. As it stands, MIN_{C_s} is a reflection of a static picture of the structure of CH_5^+, and it can be clearly described as a H_2 unit residing on top of a pyramidal CH_3^+ unit, with H_2 aligned with and slightly tilted toward one of the CH bonds of the CH_3^+ unit.

The almost unhindered permutation of the H atoms, resulting in the dynamical structure of CH_5^+, is governed by two internal motions:[24,25] the periodic (60°) "internal rotation" of the H_2 top, and the "flip" motion, whereby hydrogens are exchanged between the H_2 and CH_3 units. The transition state (TS) of the internal rotation of the H_2 unit also has C_s point-group symmetry and it is denoted here as TS_{rot}. The third SP of high distinction, denoted as TS_{flip}, is the TS structure, of C_{2v} point-group symmetry, corresponding to the flip motion. All high-level electronic-structure computations[24,25] agree that the potential energy barriers hindering these motions are very low; therefore, complete scrambling (permutation) of the hydrogens happens during the nuclear dynamics even in the ground vibrational state. Thus, one may legitimately wonder, as has been done before us,[4,6] whether CH_5^+ has a "structure" at all.

The low-energy quantum-dynamical behavior of CH_5^+ is governed by the internal rotation and flip motions. Thus, we decided to interrogate the structural preferences of the ion by asking what are the probabilities of finding the structure around the MIN_{C_s}, the TS_{rot}, and the TS_{flip} stationary points. Earlier computational studies[2,4,8,15−23] seem to agree that, despite the complete scrambling of the Hs, their motion is highly correlated in the sense that we can always identify a H_2 and a CH_3^+ unit within the actual structure.

Quantum mechanics dictates that the rovibrational eigenstates of CH_5^+ must transform according to the irreducible

Received: October 6, 2022
Published: December 19, 2022

https://doi.org/10.1021/acs.jctc.2c00991
J. Chem. Theory Comput. 2023, 19, 42−50

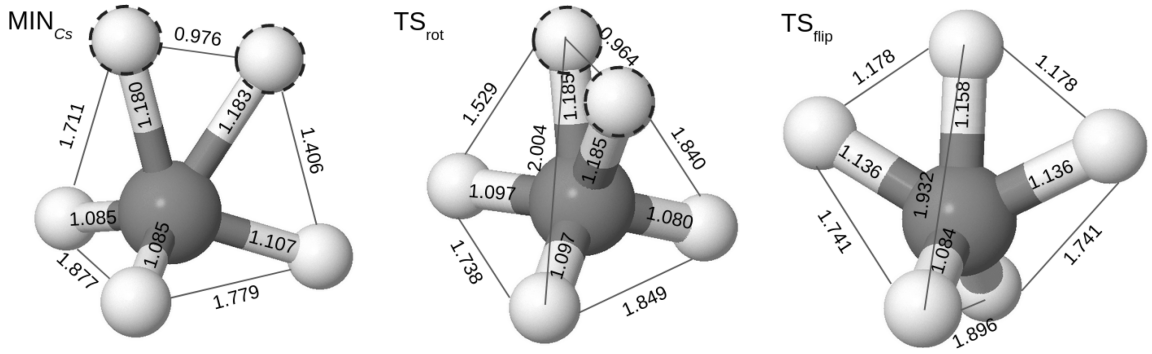

Figure 1. Structures corresponding to the three most important stationary points on the ground electronic state potential energy surface of the CH_5^+ molecular cation. The atom−atom distances, displayed in Å, are taken from ref 17. MIN_{Cs}, equilibrium structure of the global minimum; TS_{rot}, transition-state structure corresponding to the (60°) "internal rotation" of the H_2 unit; TS_{flip}, transition state structure corresponding to the flip internal motion (see text for details). Atoms of the H_2 subunit, i.e., the closest H−H pair, are denoted by dashed circles for MIN_{Cs} and TS_{rot}.

representations (irreps) of the S_5^* molecular symmetry (MS) group,[26] that the Pauli-allowed irreps of S_5^* are[23] $A_2^{\pm}$, $G_2^{\pm}$, and $H_2^{\pm}$ (this is the result of the permutation of five identical fermions), and that there are 120 versions[26,27] of the single equilibrium structure of CH_5^+. The PIMD and DQMC computational structural studies[2,8,15−17] neglected the effect of nuclear spins and thus have dealt with the totally symmetric (A_1^+) ground vibrational state, which is a state disallowed by the Pauli exclusion principle. The first allowed state, the lowest odd-parity state, LOPS, of CH_5^+ has G_2^- symmetry, and it has a relative energy of ≈10 cm^{-1}.[21−23] Thus, one must investigate the fundamental question whether there are significant differences between the effective structure of the forbidden A_1^+ ground state and that of the G_2^- LOPS.

To understand the quantum nature of the (temperature-dependent) dynamical structure of CH_5^+, the extent of the delocalization of the nuclei must also be considered. Delocalization of electrons is a well-established concept in chemistry but nuclei are often considered to be stationary (starting with the notion that they are "fixed" within the Born−Oppenheimer approximation). We investigate the delocalization of the nuclei via the computation of nuclear densities (conceptually they are similar to electron densities). Nuclear density shows the spatial distribution[28] of the nuclei in a body-fixed Cartesian-coordinate system. Hereby we calculate the nuclear densities from seven-dimensional (7D) bending-only vibrational wave functions obtained variationally, which allows the detailed study of structural preferences and the extent of nuclear delocalization, as well. It is important to emphasize that nuclear densities depend on the choice of the body-fixed frame. Introduction of a body-fixed frame is mandatory, as the vibrational wave function of an N-atomic molecule is $(3N-6)$-dimensional, and we need to specify the remaining six coordinates, describing the overall translation and rotation, to calculate the body-fixed Cartesian coordinates. In this study we principally use the Eckart embedding[29] and, as dictated by our tasks, the reference structures employed are either the MIN_{Cs}, TS_{rot}, or TS_{flip} ones. The nuclear-density plots computed this way help reveal "structural preferences", i.e., how similar the dynamical structure is to the chosen Eckart reference structure. (Note that Figure 6 of ref 8 is somewhat similar to the nuclear-density plots we present here.)

It is always enlightening to understand sophisticated variational (VAR) results via much simpler models. It is fair to say that among the models[30−39] put forward to understand qualitatively the structure, dynamics, and spectra of CH_5^+, models based on the mathematical concept of quantum graphs (QG)[40] proved to be the most successful. QGs allow to set up simple models[30,31,39] for the calculation of the lowest-energy rovibrational states of CH_5^+. Briefly, see the original publications and the Supporting Information for details, QGs are metric graphs whose vertices represent versions corresponding to a given structure with distinct numbering of the atoms, while the edges have lengths and refer to collective nuclear motions which transform the versions into each other. The QG models of CH_5^+ investigated thus far are Γ_{120}[30,39] and Γ_{60}.[31] In the case of the Γ_{120} model, there are 120 vertices, all representing versions of MIN_{Cs}; furthermore, there are 120 edges for the internal-rotation and 60 edges for the flip motions. The edge length of the flip motion turned out to be significantly shorter than that of the internal-rotation motion, $L^{rot} = 61.2\sqrt{m_e}a_0$ and $L^{flip} = 1.0\sqrt{m_e}a_0$, respectively.[30,31] The QG of the Γ_{60} model contains 60 vertices, all corresponding to versions of TS_{flip}, and its 120 edges refer to the internal rotation. The success of the Γ_{60} model[31] in representing the low-energy quantum dynamics of CH_5^+ suggests, somewhat surprisingly, that one is allowed to neglect the flip motion during the study of the low-energy dynamics of CH_5^+ (at the expense of redefining the vertices). The QG construction allows the mapping of the complex vibrational quantum dynamics of CH_5^+ onto the one-dimensional motion of a particle that can move along the edges of the quantum graph. The vibrational energy levels and wave functions are obtained by solving the one-dimensional time-independent Schrödinger equation on the QG. In the QG models of CH_5^+, the potential is assumed to be zero (the topology of the PES, that is the interconversion of versions, is included in the model through the connectivity of the graph). The QG energy levels are quantized by imposing appropriate boundary conditions on the plane-wave-like eigenstates of the free particle confined in the QG.

We employ the wave functions of the vibrational QG model[30,31] to calculate probability densities along the internal rotation and flip coordinates and to determine structural preferences this way, as well. This is also our way to answer the question whether the structural information extracted from sophisticated first-principles variational computations could be obtained from simple and even analytically solvable model(s), in this case the quantum-graph model. Whether the approach is VAR or QG, we focus on the A_1^+-symmetry ground state and

https://doi.org/10.1021/acs.jctc.2c00991
J. Chem. Theory Comput. 2023, 19, 42−50

those low-energy vibrational states whose symmetry is allowed by the Pauli exclusion principle (see Table 1, *vide infra*).

2. ALGORITHMIC DETAILS

First, we describe the algorithm how the body-fixed nuclear densities from vibrational ($J = 0$, where J is the quantum number corresponding to the overall rotation of the molecule) nuclear wave functions can be computed within the discrete variable representation (DVR)[41−43] of the nuclear Hamiltonian. Then, the way to determine probability densities along the internal rotation and flip coordinates, within the QG model, is reported.

2.1. Nuclear Density from DVR-Based Vibrational Eigenvectors. (Ro)vibrational wave functions contain all the information about effective molecular structures, but the direct analysis of multivariate wave functions is a complex task, not least because different sets of internal coordinates may correspond, when permutations of identical atoms are taken into account, to the same molecular structure. One way forward is to calculate the nuclear density, which shows the spatial distribution of the nuclei in a body-fixed Cartesian-coordinate frame (embedding). The computation of nuclear densities helps the understanding and visualization of the dynamical structure of molecules, including the (de)-localization of the nuclei. The body-fixed nuclear density can be defined the following way: if the number of nuclei of a given type in the $(x - \Delta x/2, x + \Delta x/2] \wedge (y - \Delta y/2, y + \Delta y/2] \wedge (z - \Delta z/2, z + \Delta z/2]$ domain is

Table 1. Vibrational Energy Levels of CH_5^+, with Energies Given in cm^{-1}[a]

	Vibrational energy			Structural preference			
Γ[b]	E_{VAR}	$E_{QG}^{\Gamma_{120}}$	$E_{QG}^{\Gamma_{60}}$		MIN_{Cs}	TS_{rot}	TS_{flip}
A_1^+	0.0	0.0	0.0		+	+	+
G_2^-	9.8	11.4	11.6		+	+	+
H_2^-	41.1	39.6	40.1		+	+	+
H_2^+	59.1	50.2	50.9		+	+	+
G_2^-	112.3	100.9	104.1		+	+	+
H_2^-	139.1	148.8	150.4		+	+	+
A_2^-	197.8	284.5	289.2		+	−	+
H_2^+	268.8	283.6	289.2		−	+	−
G_2^+	370.4	275.5	289.2		−	+	−
H_2^-	384.3	467.5	472.9		+	+	+
G_2^+	468.9	289.2	289.2	VAR	+	+	−
				QG	−	+	−
G_2^-	479.5	549.1	544.6		+	+	+
H_2^+	510.1	289.2	289.2	VAR	+	+	−
				QG	−	+	−
A_2^+	635.6	289.2	289.2		−	+	−

[a] E_{VAR}: 7D bending-only variational energy levels, reproduced from ref 23. $E_{QG}^{\Gamma_{120}}$ and $E_{QG}^{\Gamma_{60}}$: quantum-graph energy levels from refs 30 and 31, respectively. The "Structural preference" columns show whether the dynamical structure is similar to the given stationary-point structures (see Figure 1). The ± signs in the last three columns indicate whether there is (+) or there is no (−) structural preference for the stationary-point structure indicated in the column heading. When the structural preferences extracted from the variational (VAR) or from the quantum-graph (QG) model do not agree, the two sets of results are given in separate rows. [b] Symmetry label corresponding to the S_5^* MS group. With the exception of the A_1^+ ground state, only states allowed by the Pauli exclusion principle are listed.

$$P(x, y, z) = \varrho(x, y, z)\Delta x\Delta y\Delta z \tag{1}$$

then $\varrho(x, y, z)$ is the body-fixed nuclear density and x, y, and z are Cartesian coordinates. It is important to use an embedding because we must separate the overall rotation and translation as we are interested in structural changes. There can be many different physically sensible embeddings for a given system, which result in different nuclear-density plots. In principle, the structural information obtained from the different embeddings should not be contradictory but complementary. Nevertheless, it is important to appreciate that nuclear density plots strongly depend on the chosen embedding. For example, if we plot the nuclear density of H_2O in the bisector embedding (with the HOH bisector on the z axis), the densities of the two Hs will be "symmetric" (with respect to z), while if we use an OH embedding, then one hydrogen is restricted to the z axis, and the other will be delocalized in the molecular plane.

In this study, probability densities of different structures are extracted from reduced-dimensional vibrational wave functions of CH_5^+ (see ref 23 for further details, where the seven-dimensional (7D) bending-only vibrational states have also been computed with the in-house code GENIUSH[23,44,45]). The vibrational basis in GENIUSH is the direct product of $\chi_{n_k}(q_k)$ one-dimensional discrete variable representation (DVR) basis functions, where $\chi_{n_k}(q_k)$ is the n_kth DVR basis function for the q_k ($k = 1, ..., D$) coordinate and $D \leq 3N - 6$ is the number of active internal coordinates (the remaining $3N - 6 - D$ coordinates are fixed). The vibrational wave function is then written as

$$\Psi^{int}(q_1, ..., q_D) = \sum_{n_1,...,n_D=1}^{N_1,...,N_D} c_{n_1,...,n_D} \prod_{k=1}^{D} \chi_{n_k}(q_k) \tag{2}$$

where N_k is the number of basis functions used for the q_k coordinate and $c_{n_1, ..., n_D}$ are expansion coefficients. We can calculate the integral of the absolute square of the wave function utilizing the DVR quadrature rules:

$$1 = \int_{min_1}^{max_1} \cdots \int_{min_D}^{max_D} |\Psi^{int}(q_1, ..., q_D)|^2 dq_1 \ldots dq_D = \sum_{n_1,...,n_D=1}^{N_1,...,N_D} |\Psi^{int}(q_{1,n_1}, ..., q_{D,n_D})|^2 w_{1,n_1} \ldots w_{D,n_D}, \tag{3}$$

where min_k and max_k are the lower and upper boundaries of coordinate q_k, respectively, q_{k,n_k} is the n_kth DVR quadrature point of the q_k coordinate, and w_{k,n_k} is the corresponding DVR weight. The ith DVR function is nonzero only at the ith grid point and zero at all the other grid points (discrete Dirac-delta property):

$$\chi_{k,i}(q_{k,j}) = \delta_{ij} w_{k,i}^{-1/2} \tag{4}$$

Therefore, the wave function at a given grid point becomes

$$\Psi^{int}(q_{1,n_1}, ..., q_{D,n_D}) = c_{n_1,...,n_D} \prod_{k=1}^{D} w_{k,n_k}^{-1/2} \tag{5}$$

and

$$|c_{n_1,...,n_D}|^2 = |\Psi^{int}(q_{1,n_1}, ..., q_{D,n_D})|^2 \prod_{k=1}^{D} w_{k,n_k} \tag{6}$$

From this and eq 3, we obtain

https://doi.org/10.1021/acs.jctc.2c00991
J. Chem. Theory Comput. 2023, 19, 42−50

$$1 = \int_{\min_1}^{\max_1} \cdots \int_{\min_D}^{\max_D} |\Psi^{\text{int}}(q_1, \ldots, q_D)|^2 \, dq_1 \ldots dq_D = \sum_{n_1,\ldots,n_D=1}^{N_1,\ldots,N_D} |c_{n_1,\ldots,n_D}|^2 \tag{7}$$

This shows that the probability of finding the molecular structure in the proximity of $(q_{1,n_1}, \ldots, q_{D,n_D})$ is $|c_{n_1,\ldots,n_D}|^2$, where "proximity" can be defined as a region with a volume element $w_{1,n_1} \ldots w_{D,n_D}$ [*cf.* eqs 6 and 3].

In order to calculate the nuclear density, we have to transform the internal coordinates to body-fixed Cartesian coordinates. The actual values of the $q_1, \ldots, q_D$ active coordinates, the values of the $q_{D+1}, \ldots, q_{3N-6}$ fixed coordinates, and the chosen embedding determine the $x_1,y_1,z_1, \ldots, x_N,y_N,z_N$ Cartesian coordinates of the nuclei. During the calculation of the nuclear density, we set up a three-dimensional Cartesian grid with Δx, Δy, and Δz step sizes. The probability of finding the ith nucleus with coordinates (x_i, y_i, z_i) in the "box" corresponding to the Cartesian grid point (x, y, z) is

$$p_i(x, y, z) \approx \sum_{n_1,\ldots,n_D \in S_i} |c_{n_1,\ldots,n_D}|^2 \tag{8}$$

where S_i denotes those $n_1, \ldots, n_D$ index sets of the DVR grid for which $x_i \in (x - \Delta x/2, x + \Delta x/2]$, $y_i \in (y - \Delta y/2, y + \Delta y/2]$, and $z_i \in (z - \Delta z/2, z + \Delta z/2]$. Therefore, the number of nuclei of a given type in this region is

$$P(x, y, z) = \sum_{j=1}^{M} \sum_i p_i^j(x, y, z) \tag{9}$$

where i denotes the nucleus of the given type, while j stands for the components of a multiply degenerate state that transforms as a M-dimensional irrep of the molecular symmetry (MS) group, and p_i^j is calculated from the $c^j_{n_1,\ldots,n_D}$ DVR-coefficients of the jth component of the multiply degenerate state according to eq 8. Then, the nuclear density at the Cartesian grid point (x,y,z) is calculated as

$$\varrho(x, y, z) \approx \frac{\sum_{j=1}^{M} \sum_i \sum_{n_1,\ldots,n_D \in S_i} |c^j_{n_1,\ldots,n_D}|^2}{\Delta x \Delta y \Delta z} \tag{10}$$

In this study, we chose to use the Eckart embedding and the reference structures employed include the MIN_{Cs} and the TS_{rot} and TS_{flip} transition-state structures. We used the method of ref 46 to rotate the molecular structure to the Eckart frame. The nuclear-density plots computed this way convey information about "structural preferences," i.e., how similar the dynamical structure is to the given Eckart reference structure. Permutation of the Hs needs to be taken into account during the calculation of the nuclear density, because the result of the Eckart rotation is sensitive to the order of the H atoms, since we rotate the ith atom of the actual distorted structure to the ith atom of the reference. In the wave function, the different versions of a given structure correspond to different sets of internal coordinates, but they should have the same body-fixed Cartesian coordinates in the nuclear-density plot. The reference structure corresponds to a single version, but when we sum the density contributions of the distorted structures, each distorted structure appears many times with different numberings of the atoms, so in each case we renumber the hydrogen atoms to get the best agreement with the reference structure after the Eckart rotation.

2.2. Probability Density along the Permutational Coordinates, Calculated from the Quantum-Graph Model. We have calculated the probability density of the structures along the internal rotation or the flip permutational coordinates (edges of the QG) from the Γ_{120}[30] and Γ_{60}[31] QG wave functions. The probability density of finding the particle at position x on edge e of the QG is $|\Psi_e(x)|^2$, where $\Psi_e(x)$ is a QG eigenfunction along e. If we define a reaction path corresponding to the permutation of the Hs, we can map this point of the QG to a unique structure of CH_5^+, whereby the numbering of the atoms is determined by the versions at the two vertices connected by e. If the length of the edge is L, then the $x = 0$ and $x = L$ positions are mapped to versions of the structure at the vertices, while $x = L/2$ is mapped to versions of the transition-state structure of the given internal motion. However, if we do not consider the numbering of the atoms, there will be other points of the graph which correspond to the same structure as x on edge e. These symmetry-equivalent points can be obtained via acting by the elements of S_5 (symmetric group of degree five) on point x of edge e, when a point on a given type of edge (internal rotation or flip) is mapped onto an edge of the same type. Note that we use S_5 and not the full MS group S_5^*. This is done because the inversion operator may transform the molecule to a structure that is not superimposable with the original one using rotations, even if we do not consider the numbering of the atoms.

Therefore, the probability density of the internal rotation or flip coordinate is

$$p_{\text{rot/flip}}(x) = \frac{1}{M} \sum_{i=1}^{M} \sum_{\hat{g} \in S_5} |\Psi^i_{\text{rot/flip}}(\hat{g}x)|^2 = \frac{1}{M} \sum_{i=1}^{M} \sum_{\hat{g} \in S_5} |\hat{g}^{-1}\Psi^i_{\text{rot/flip}}(x)|^2 \tag{11}$$

where i denotes components of a multiply degenerate state transforming as an M-dimensional irrep, and "rot/flip" denotes a selected internal rotation or flip edge. We will use the last expression of eq 11 to calculate the probability density. The effect of $\hat{g}$ on the wave function can be obtained by employing a $\mathbf{U}$ unitary matrix of dimension $M \times M$:

$$\hat{g}\Psi^i_e(x) = \sum_{j=1}^{M} U_{ij}\Psi^j_e(x) \tag{12}$$

Using the properties of the unitary matrix, we obtain

$$\sum_{i=1}^{M} |\hat{g}\Psi^i_e(x)|^2 = \sum_{i=1}^{M} |\Psi^i_e(x)|^2 \tag{13}$$

for any $\hat{g} \in S_5$. Therefore,

$$p_{\text{rot/flip}}(x) = \frac{120}{M} \sum_{i=1}^{M} |\Psi^i_{\text{rot/flip}}(x)|^2 \tag{14}$$

where we used the fact that S_5 has 120 elements.

Therefore, the probability density of the internal rotation coordinate is

https://doi.org/10.1021/acs.jctc.2c00991
J. Chem. Theory Comput. 2023, 19, 42−50

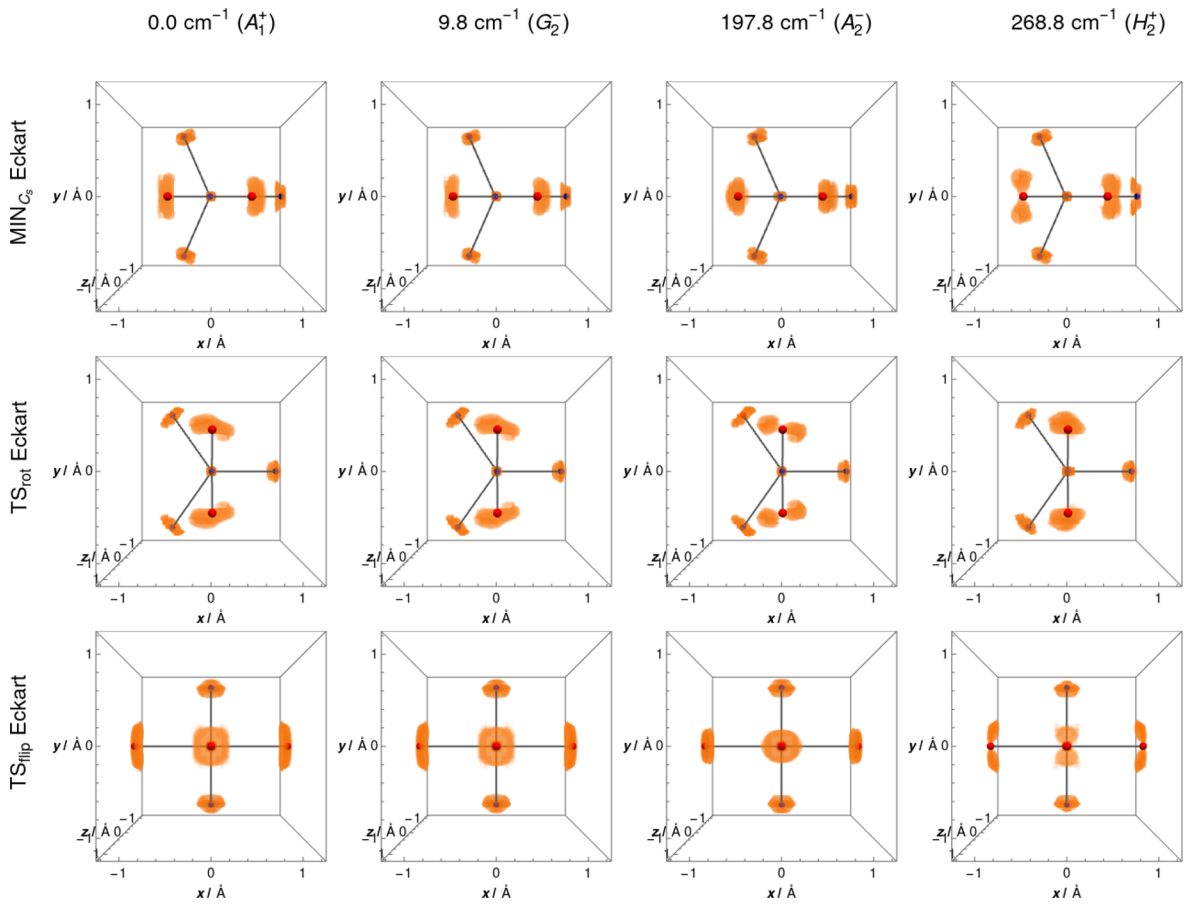

Figure 2. Body-fixed nuclear density for four selected vibrational states of CH_5^+ (four columns), calculated from variational wave functions (see Supporting Information for the figures corresponding to other states). The body-fixed frame chosen is the Eckart frame, where the reference structure is either MIN$_{Cs}$ (first row), TS$_{rot}$ (second row), or TS$_{flip}$ (third row). The orange-colored regions correspond to about 85% probability, while the reference structures are shown in wireframe, where the H atoms of the H_2 unit are red and the H atoms of the CH_3^+ unit are blue. Note that there is no large-scale *spatial* nuclear delocalization. The plots also show the structural preference, i.e., if there is a high probability of finding the molecular structure in the given reference structure. For example, the nuclear density for the 197.8 cm^{-1} (A_2^-) state is large around the MIN$_{Cs}$ and TS$_{flip}$ reference structures, so these structures are preferred, while it is zero in the TS$_{rot}$ reference structure, so this structure is avoided.

$$p_{\text{rot}}(x) = \frac{120}{M}\sum_{i=1}^{M}|\Psi^i_{\text{rot}}(x)|^2 = \frac{1}{M}\sum_{i=1}^{M}\sum_{r\in\text{rot}}|\Psi^i_r(x)|^2 \tag{15}$$

with $x \in [0, L^{\text{rot}})$ and

$$p_{\text{flip}}(x) = \frac{120}{M}\sum_{i=1}^{M}|\Psi^i_{\text{flip}}(x)|^2 = \frac{2}{M}\sum_{i=1}^{M}\sum_{f\in\text{flip}}|\Psi^i_f(x)|^2 \tag{16}$$

where the factor 2 for $p_{\text{flip}}(x)$ is needed because there are only 60 flip edges, and the r and f indices denote all internal rotation and flip edges, respectively. In the case of $p_{\text{flip}}(x)$, the range of x is either $[0, L^{\text{flip}}/2]$ or $[L^{\text{flip}}/2, L^{\text{flip}}]$, though the former is more natural, because in Γ_{120} the x and the $L^{\text{flip}} - x$ positions on a flip edge are mapped to the same structure if we do not consider the numbering of the atoms.

The norm of the QG wave function is calculated as

$$1 = \langle\Psi^i|\Psi^i\rangle = \sum_{r\in\text{rot}}\int_0^{L^{\text{rot}}}|\Psi^i_r(x)|^2\,\mathrm{d}x + \sum_{f\in\text{flip}}\int_0^{L^{\text{flip}}}|\Psi^i_f(x)|^2\,\mathrm{d}x \tag{17}$$

Combining eq 17 with eqs 15 and 16, and using $p_{\text{flip}}(x) = p_{\text{flip}}(L^{\text{flip}} - x)$, we obtain that the sum of the integrals of $p_{\text{flip}}(x)$ and $p_{\text{rot}}(x)$ is 1, as expected,

$$\int_0^{L^{\text{flip}}/2}p_{\text{flip}}(x)\,\mathrm{d}x + \int_0^{L^{\text{rot}}}p_{\text{rot}}(x)\,\mathrm{d}x = 1 \tag{18}$$

3. RESULTS AND DISCUSSION

3.1. Nuclear Density from Variational Wave Functions. Figure 2 shows the body-fixed nuclear density for four selected vibrational states, calculated from VAR wave functions, while the nuclear density for the other states can be found in the Supporting Information. As already discussed, nuclear densities are always specified in a certain body-fixed frame and the body-fixed coordinate axes applied in this study follow the internal rotation and flip motions of CH_5^+. In addition, probabilities of finding identical nuclei (H atoms in this case) are summed up and evaluated in a three-dimensional Cartesian grid. The orange color of Figure 2 indicates the region of space in which the H atoms can be found with about 85% probability.

The nuclear-density plots clearly show the structural preferences of the vibrational states. For all four states shown, the H atoms are localized near the reference positions,

https://doi.org/10.1021/acs.jctc.2c00991
J. Chem. Theory Comput. 2023, 19, 42−50

which implies that the difference of the equilibrium and TS structures is comparable to the extent of nuclear delocalization (see the Supporting Information on how to quantify the similarity of molecular structures). When the orange regions of the plot form circular spots around the reference nuclear positions, we may say that the dynamical structure is similar to the given reference structure, or, in other words, the wave function has large amplitude around the given reference structure. Note that the structural preference is not "exclusive" in the sense that there can be preference for multiple structures. For example, the vibrational wave functions of the (Pauli-forbidden) A_1^+ ground state and the G_2^- LOPS state, the latter at a relative energy of 10 cm^{-1}, have significant amplitude at the MIN_{Cs}, TS_{rot}, and TS_{flip} structures. The nuclear densities of the A_1^+ ground state and the LOPS are very similar. This is related to the fact that the energy of the LOPS is close to that of the ground state. A more conclusive rationalization will be outlined in the section where the QG results are presented (see also the Supporting Information). In summary, the results obtained for the LOPS support the earlier picture established for the Pauli-forbidden A_1^+-symmetry ground state: despite the pronounced scrambling of the H atoms, the local dynamical structure of CH_5^+ is a well-defined CH_3^+ tripod with a H_2 unit on top, with surprisingly modest delocalization of the nuclei. Note, finally, that we can safely assume that at the temperature of the spectroscopic experiments, 4−10 K,[10,13] only the LOPS state has a significant population, as the next Pauli-allowed state is the $J = 1$ G_2^+ state at 23 cm^{-1} above the Pauli-forbidden ground state.[22]

In some cases the nuclear density is zero or very small at the reference position of certain H atoms (in such cases the shape of the orange spots is similar to the numeral 8). Then we can say that the dynamical structure is not similar to the chosen reference structure. This is the case for the 268.8 cm^{-1} (H_2^+) state and the MIN_{Cs} and TS_{flip} reference structures, and, as dictated by symmetry, the 197.8 cm^{-1} (A_2^-) state and the TS_{rot} reference structure.

Figure 2 shows only four selected states; the structural preferences of other Pauli-allowed states are summarized in Table 1, where the ± signs in the last three columns indicate whether there is (+) or there is no (−) structural preference for the stationary-point structure indicated in the column heading. Based on all these results one can conclude that the nuclear density of the first six vibrational states, all significantly below 200 cm^{-1}, is very similar to that of the ground state; the wave functions have large amplitude around all SP structures, while there are certain higher-energy states which tend to avoid certain SP structures. Even though the structural preferences of the different vibrational states are not the same, the extent of nuclear delocalization does not change significantly with the energy. The somewhat complex explanation of these observations will be given next, based on QG results.

3.2. Probability Densities along the Permutational Coordinates, Calculated from the Quantum-Graph Model. Panel a of Figure 3 shows the probability densities $p_{rot}(x)$ and $p_{flip}(x)$ along the internal rotation and flip edges, respectively, calculated from QG wave functions. Here, the permutational coordinate x denotes a point on the edge. This x should not to be confused with Cartesian coordinate x used in the nuclear density calculation. If we define a reaction path, we can map point x of an edge to a unique structure of CH_5^+ (see the structures at the top of Figure 3a). Figure 3 displays results calculated from the wave functions of the Γ_{120} QG model,[30]

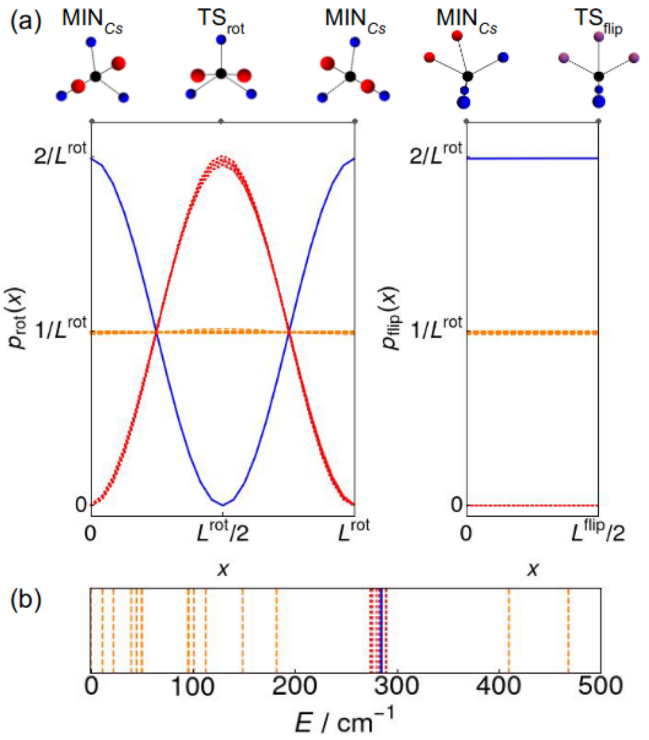

Figure 3. (a) Probability density of the internal rotation and flip permutational coordinates, calculated from the Γ_{120}[30] quantum-graph (QG) model. Here, the permutational coordinate x denotes a point on the edge of the QG, not to be confused with the x Cartesian coordinate used in the nuclear-density calculation. The $x = 0$ and $x = L^{rot}$ points correspond to MIN_{Cs}, while $x = L^{rot}/2$ and $x = L^{flip}/2$ correspond to TS_{rot} and TS_{flip}, respectively (see structures at the top). (b) Vibrational energy levels from the Γ_{120} model (see Table S1 of the Supporting Information for the energy values). The color-coding of panels (a) and (b) are the same; therefore, we see that shapes of the probability densities are determined by the energy. If the energy is between 270 and 290 cm^{-1}, then $p_{rot} \propto \sin^2(x\pi/L^{rot})$ (several red dotted curves), except for the 284.5 cm^{-1} (A_2^-) state (single blue curve), for which $p_{rot} \propto \cos^2(x\pi/L^{rot})$, while for other energies shown here p_{rot} is constant (several orange dashed curves). If p_{rot} or p_{flip} is large for x values corresponding to MIN_{Cs}, TS_{rot}, or TS_{flip}, then there is a high probability of finding the molecular structure at the given structure. For example, in the case of the 284.5 cm^{-1} (A_2^-) state (single blue curve), p_{rot} and p_{flip} are large for points corresponding to MIN_{Cs} and TS_{flip}, so there is a structural preference for these structures, while p_{rot} is very small at $L^{rot}/2$ so TS_{rot} is avoided.

while the highly similar figures obtained from the Γ_{60} model[31] can be found in the Supporting Information. Figure 3 is based on all vibrational states, including the Pauli-forbidden ones, up to 500 cm^{-1} in relative energy (see the Supporting Information for a full list of Γ_{120} and Γ_{60} QG vibrational energies).

The structural preferences given in Table 1 can be ascertained from $p_{rot}(x)$ and $p_{flip}(x)$ as follows. If the probability density is large at a value x, corresponding to a SP structure, we say that there is preference for the chosen SP structure. First, let us discuss the probability density along the internal rotation for the Γ_{120} model with $E_{QG}^{\Gamma_{120}}$ energies (see Table 1). There are three qualitatively different densities: (*i*) for all but one state with energies between 270 and 290 cm^{-1} (red dotted curves in Figure 3), $p_{rot}(x) \approx 2/L^{rot} \sin^2(x\pi/L^{rot})$, which means that MIN_{Cs} is avoided and TS_{rot} is preferred; (*ii*) in the case of the 284.5 cm^{-1} (A_2^-) state (blue curve), $p_{rot}(x) \approx 2/L^{rot} \cos^2(x\pi/L^{rot})$, which means that the structure is similar

https://doi.org/10.1021/acs.jctc.2c00991
J. Chem. Theory Comput. 2023, 19, 42−50

to MIN_{Cs} but avoids TS_{rot}; and (*iii*) for the other states studied here (orange dashed curves), the $p_{rot}(x)$ density is almost constant, $p_{rot}(x) \approx 1/L^{rot}$. The situation is very similar for the Γ_{60} model, but states of the Γ_{120} model, where, in cm^{-1}, $270 < E_{QG}^{\Gamma_{120}} < 290$, become degenerate with an energy of 289.2 cm^{-1}.

The observations made are fully supported by analytical derivations, presented in the Supporting Information, possible for the Γ_{60} QG model. If $E_{QG}^{\Gamma_{60}} = (n\pi/L^{rot})^2/2$, then the probability density along the internal-rotation edge is $p_{rot}(x) = 2/L^{rot} \sin^2(xn\pi/L^{rot})$ for all states except one, for which $p_{rot}(x) = 2/L^{rot} \cos^2(xn\pi/L_{rot})$, while for other energy values the probability density is constant, $p_{rot}(x) = 1/L^{rot}$. The conclusions are the same for Γ_{120}, as $L^{flip} \ll L^{rot}$, but the $\sin^2$- and $\cos^2$-type probability densities are not restricted to certain energy values but appear in regions close to $E_{QG}^{\Gamma_{120}} = (n\pi/L^{rot})^2/2$.

For the Γ_{120} model, Figure 3 also shows the probability densities along the flip edge. In this case x is limited to the range of $[0, L^{flip}/2]$ because the x and the $L^{flip}-x$ positions on a given edge are mapped to the same structure (not considering the numbering of the atoms). The $p_{flip}(x)$ densities show strong correlation with the densities along the internal rotation. The densities along the flip edge are nearly constant for all states studied here with $p_{flip}(x) \approx p_{rot}(0)$. This means that for the 284.5 cm^{-1} (A_2^-) state and for states whose energy is *not* between 270 and 290 cm^{-1}, there is a high probability of finding the structure at MIN_{Cs} and TS_{flip}, as well. For the other states, whose energy is between 270 and 290 cm^{-1}, the probability density along the flip edge is almost zero; therefore, the amplitude of the wave function is very small in MIN_{Cs} and TS_{flip}. These results show that within the QG model the probability density of the flip and the internal rotation is determined by the energy of the state.

3.3. Comparison of the Structural Preferences Obtained from Variational Wave Functions and the Quantum-Graph Models. Table 1 shows the vibrational energies, calculated with different methods, as well as the "structural preferences" of each state. The QG and the VAR energy levels were matched based on the symmetry and the energy order. The two sets of energy levels show excellent agreement below 150 cm^{-1}, because the QG edge lengths were fitted to these energies, while there are significant differences for the higher-lying states. The structural information gained from the VAR wave functions and the QG model agree for all states, except for two high-energy cases, the 468.9 cm^{-1} (G_2^+) and the 510.1 cm^{-1} (H_2^+) states. Note that we can observe agreement in the structural preferences for most higher-lying states, as well, even when the QG and the VAR energies are very different. Therefore, the QG model is not only suitable to predict the low-lying rovibrational energy levels of CH_5^+, but it also provides sensible structural information, and the analysis of the probability densities along the edges corresponding to the permutational coordinates is straightforward and supports the not so obvious interpretation of the nuclear-density plots.

4. SUMMARY AND CONCLUSIONS

The dynamical structure of CH_5^+, a molecular cation that undergoes complex nuclear dynamics, has been studied. Structural preference is defined by how similar the dynamical structure is to the MIN_{Cs}, TS_{rot}, and TS_{flip} stationary-point structures (see Figure 1). Body-fixed nuclear-density plots from variational vibrational wave functions and probability densities of the internal rotation and flip coordinates from wave functions of the quantum-graph (QG) model reveal the same structural preferences. This holds even for higher-energy states, where the variational and the quantum-graph energies are rather different. Most states have a preference for multiple stationary-point structures, suggesting that the difference of the equilibrium and transition-state structures is comparable to the extent of nuclear delocalization. However, the nuclear-density plots show that the *spatial* delocalization is not large for the states studied here and that it does not increase even for the higher-lying states. One important result is that the dynamical structures of the Pauli-forbidden A_1^+ ground state and the lowest Pauli-allowed state, at ≈10 cm^{-1} above the zero-point energy,[21−23] look identical. In fact, the dynamical structures of the first six vibrational states are very similar. Another very important result of the present study is that in the QG model the probability densities of the permutational coordinates are determined by state energies. We can rationalize different shapes of the density by analytical derivations (see Supporting Information): for certain energy values, when $E_{QG}^{\Gamma_{60}} = (n\pi/L^{rot})^2/2$, the probability density along the internal rotation is $p_{rot}(x) \propto \sin^2(xn\pi/L^{rot})$ for all states except one, for which $p_{rot}(x) \propto \cos^2(xn\pi/L^{rot})$, while for other energy values $p_{rot}(x)$ is constant.

■ ASSOCIATED CONTENT

Supporting Information

The Supporting Information is available free of charge at https://pubs.acs.org/doi/10.1021/acs.jctc.2c00991.

> Quantification of the similarity of molecular structures, the full set of nuclear-density plots obtained from variational computations, the full set of quantum-graph vibrational energy levels, and analytical derivation of the relationship between the quantum-graph energies and the probability densities along the permutational coordinates (PDF)

■ AUTHOR INFORMATION

Corresponding Author

Attila G. Császár − *Laboratory of Molecular Structure and Dynamics, Institute of Chemistry, ELTE Eötvös Loránd University, H-1117 Budapest, Hungary; MTA-ELTE Complex Chemical Systems Research Group, H-1518 Budapest 112, Hungary;* orcid.org/0000-0001-5640-191X; Email: attila.csaszar@ttk.elte.hu

Authors

Irén Simkó − *Hevesy György PhD School of Chemistry, ELTE Eötvös Loránd University, H-1117 Budapest, Hungary; Laboratory of Molecular Structure and Dynamics, Institute of Chemistry, ELTE Eötvös Loránd University, H-1117 Budapest, Hungary; MTA-ELTE Complex Chemical Systems Research Group, H-1518 Budapest 112, Hungary*

Csaba Fábri − *MTA-ELTE Complex Chemical Systems Research Group, H-1518 Budapest 112, Hungary;* orcid.org/0000-0001-9746-1548

Complete contact information is available at: https://pubs.acs.org/10.1021/acs.jctc.2c00991

Notes

The authors declare no competing financial interest.

https://doi.org/10.1021/acs.jctc.2c00991
J. Chem. Theory Comput. 2023, 19, 42−50

■ ACKNOWLEDGMENTS

The authors are grateful to the National Research, Development and Innovation Fund (NKFIH) for support (grant no. K138233). IS was supported by the ÚNKP-21-3 New National Excellence Program of the Ministry for Innovation and Technology, supported by NKFIH.

■ REFERENCES

(1) Császár, A. G.; Fábri, C.; Sarka, J. Quasistructural molecules. *WIREs Comput. Mol. Sci.* **2020**, *10*, e1432.
(2) Marx, D.; Parrinello, M. Structural quantum effects and three−centre two−electron bonding in CH_5^+. *Nature* **1995**, *375*, 216−218.
(3) Marx, D.; Savin, A. Topological bifurcation analysis: Electronic structure of CH_5^+. *Angew. Chem., Int. Ed.* **1997**, *36*, 2077−2080.
(4) Schreiner, P. R. Does CH_5^+ have (a) "structure"? A tough test for experiment and theory. *Angew. Chem., Int. Ed.* **2000**, *39*, 3239−3241.
(5) Oka, T. Taming CH_5^+, the "enfant terrible" of chemical structures. *Science* **2015**, *347*, 1313−1314.
(6) Scuseria, G. E. The elusive signature of CH_5^+. *Nature* **2015**, *366*, 512−513.
(7) Kramer, G. M.; Oka, T.; White, E. T.; Marx, D.; Parrinello, M. CH_5^+ stability and mass spectrometry. *Science* **1999**, *286*, 1051−1051.
(8) Thompson, K. C.; Crittenden, D. L.; Jordan, M. J. T. CH_5^+: Chemistry's chameleon unmasked. *J. Am. Chem. Soc.* **2005**, *127*, 4954−4958.
(9) White, E. T.; Tang, J.; Oka, T. CH_5^+: the infrared spectrum observed. *Science* **1999**, *284*, 135−137.
(10) Asvany, O.; Padma Kumar, P.; Redlich, B.; Hegemann, I.; Schlemmer, S.; Marx, D. Understanding the infrared spectrum of bare CH_5^+. *Science* **2005**, *309*, 1219−1222.
(11) Huang, X.; McCoy, A. B.; Bowman, J. M.; Johnson, L. M.; Savage, C.; Dong, F.; Nesbitt, D. J. Quantum deconstruction of the infrared spectrum of CH_5^+. *Science* **2006**, *311*, 60−63.
(12) Ivanov, S. D.; Asvany, O.; Witt, A.; Hugo, E.; Mathias, G.; Redlich, B.; Marx, D.; Schlemmer, S. Quantum-induced symmetry breaking explains infrared spectra of CH_5^+ isotopologues. *Nat. Chem.* **2010**, *2*, 298−302.
(13) Asvany, O.; Yamada, K. M. T.; Brünken, S.; Potapov, A.; Schlemmer, S. Experimental ground-state combination differences of CH_5^+. *Science* **2015**, *347*, 1346−1349.
(14) Brackertz, S.; Schlemmer, S.; Asvany, O. Searching for new symmetry species of CH_5^+ − From lines to states without a model. *J. Mol. Spectrosc.* **2017**, *342*, 73−82.
(15) McCoy, A. B.; Braams, B. J.; Brown, A.; Huang, X.; Jin, Z.; Bowman, J. M. Ab initio diffusion Monte Carlo calculations of the quantum behavior of CH_5^+ in full dimensionality. *J. Phys. Chem. A* **2004**, *108*, 4991−4994.
(16) Johnson, L. M.; McCoy, A. B. Evolution of structure in CH_5^+ and its deuterated analogues. *J. Phys. Chem. A* **2006**, *110*, 8213−8220.
(17) Brown, A.; McCoy, A. B.; Braams, B. J.; Jin, Z.; Bowman, J. M. Quantum and classical studies of vibrational motion of CH_5^+ on a global potential energy surface obtained from a novel *ab initio* direct dynamics approach. *J. Chem. Phys.* **2004**, *121*, 4105−4116.
(18) Hinkle, C. E.; McCoy, A. B. Characterizing excited states of CH_5^+ with diffusion Monte Carlo. *J. Phys. Chem. A* **2008**, *112*, 2058−2064.
(19) Hinkle, C. E.; Petit, A. S.; McCoy, A. B. Diffusion Monte Carlo studies of low energy ro-vibrational states of CH_5^+ and its deuterated isotopologues. *J. Mol. Spectrosc.* **2011**, *268*, 189−198.
(20) Wodraszka, R.; Manthe, U. CH_5^+: Symmetry and the entangled rovibrational quantum states of a fluxional molecule. *J. Phys. Chem. Lett.* **2015**, *6*, 4229−4232.
(21) Wang, X.-G.; Carrington, T., Jr. Vibrational energy levels of CH_5^+. *J. Chem. Phys.* **2008**, *129*, 234102.
(22) Wang, X.-G.; Carrington, T. Calculated rotation-bending energy levels of CH_5^+ and a comparison with experiment. *J. Chem. Phys.* **2016**, *144*, 204304.
(23) Fábri, C.; Quack, M.; Császár, A. G. On the use of nonrigid-molecular symmetry in nuclear-motion computations employing a discrete variable representation: a case study of the bending energy levels of CH_5^+. *J. Chem. Phys.* **2017**, *147*, 134101.
(24) Schreiner, P. R.; Kim, S.-J.; Schaefer, H. F.; Schleyer, P. v. R. CH_5^+: The never-ending story or the final word? *J. Chem. Phys.* **1993**, *99*, 3716−3720.
(25) Müller, H.; Kutzelnigg, W.; Noga, J.; Klopper, W. CH_5^+: The story goes on. An explicitly correlated coupled-cluster study. *J. Chem. Phys.* **1997**, *106*, 1863−1869.
(26) Bunker, P. R.; Jensen, P. *Molecular Symmetry and Spectroscopy*; NRC Research Press: Ottawa, 2006.
(27) Longuet-Higgins, H. C. The symmetry groups of non-rigid molecules. *Mol. Phys.* **1963**, *6*, 445−460.
(28) Kusalik, P. G.; Svishchev, I. M. The spatial structure in liquid water. *Science* **1994**, *265*, 1219−1221.
(29) Louck, J. D.; Galbraith, H. W. Eckart vectors, Eckart frames, and polyatomic molecules. *Rev. Mod. Phys.* **1976**, *48*, 69−106.
(30) Fábri, C.; Császár, A. G. Vibrational quantum graphs and their application to the quantum dynamics of CH_5^+. *Phys. Chem. Chem. Phys.* **2018**, *20*, 16913−16917.
(31) Rawlinson, J. I.; Fábri, C.; Császár, A. G. Exactly solvable 1D model explains the low-energy vibrational level structure of protonated methane. *Chem. Commun.* **2021**, *57*, 4827−4830.
(32) Bunker, P. R.; Ostojic, B.; Yurchenko, S. A theoretical study of the millimeterwave spectrum of CH_5^+. *J. Mol. Struct.* **2004**, *695*−*696*, 253−261.
(33) Deskevich, M. P.; McCoy, A. B.; Hutson, J. M.; Nesbitt, D. J. Large-amplitude quantum mechanics in polyatomic hydrides. II. A particle-on-a-sphere model for XH_n (n = 4,5). *J. Chem. Phys.* **2008**, *128*, 094306.
(34) Uhl, F.; Walewski, L.; Forbert, H.; Marx, D. Adding flexibility to the "particles-on-a-sphere" model for large-amplitude motion: POSflex force field for protonated methane. *J. Chem. Phys.* **2014**, *141*, 104110.
(35) Schmiedt, H.; Schlemmer, S.; Jensen, P. Symmetry of extremely floppy molecules: Molecular states beyond rotation-vibration separation. *J. Chem. Phys.* **2015**, *143*, 154302.
(36) Schmiedt, H.; Jensen, P.; Schlemmer, S. Collective molecular superrotation: A model for extremely flexible molecules applied to protonated methane. *Phys. Rev. Lett.* **2016**, *117*, 223002.
(37) Schmiedt, H.; Jensen, P.; Schlemmer, S. The role of angular momentum in the superrotor theory for rovibrational motion of extremely flexible molecules. *J. Mol. Spectrosc.* **2017**, *342*, 132−137.
(38) Schmiedt, H.; Jensen, P.; Schlemmer, S. Rotation-vibration motion of extremely flexible molecules − The molecular superrotor. *Chem. Phys. Lett.* **2017**, *672*, 34−46.
(39) Rawlinson, J. I. Quantum graph model for rovibrational states of protonated methane. *J. Chem. Phys.* **2019**, *151*, 164303.
(40) Berkolaiko, G.; Kuchment, P. Introduction to Quantum Graphs. In *Mathematical Surveys and Monographs*; American Mathematical Society, 2013; Vol. *186*.
(41) Harris, D. O.; Engerholm, G. G.; Gwinn, W. D. Calculation of matrix elements for one-dimensional quantum-mechanical problems and the application to anharmonic oscillators. *J. Chem. Phys.* **1965**, *43*, 1515−1517.
(42) Light, J. C.; Carrington, T. Discrete variable representations and their utilization. *Adv. Chem. Phys.* **2000**, *114*, 263−310.
(43) Beck, M. H.; Jäckle, A.; Worth, G. A.; Meyer, H.-D. The multiconfiguration time-dependent Hartree method: a highly efficient algorithm for propagating wavepackets. *Phys. Rep.* **2000**, *324*, 1−105.
(44) Fábri, C.; Mátyus, E.; Császár, A. G. Rotating full- and reduced-dimensional quantum chemical models of molecules. *J. Chem. Phys.* **2011**, *134*, 074105.
(45) Mátyus, E.; Czakó, G.; Császár, A. G. Toward black-box-type full- and reduced-dimensional variational (ro)vibrational computations. *J. Chem. Phys.* **2009**, *130*, 134112.

https://doi.org/10.1021/acs.jctc.2c00991
J. Chem. Theory Comput. 2023, 19, 42−50

(46) Krasnoshchekov, S. V.; Isayeva, E. V.; Stepanov, N. F. Determination of the Eckart molecule-fixed frame by use of the apparatus of quaternion algebra. *J. Chem. Phys.* **2014**, *140*, 154104.

https://doi.org/10.1021/acs.jctc.2c00991
J. Chem. Theory Comput. 2023, 19, 42−50